Zero-Field J-spectroscopy of Quadrupolar Nuclei

Danila A. Barskiy,*[,a,b,c,d] John W. Blanchard,[c,d] Moritz Reh,[e] Tobias Sjoelander,[a,b]

Alexander Pines,[a,b] and Dmitry Budker,[c,d,e]

[a]Department of Chemistry, University of California - Berkeley, California 94720-3220, USA

[b]Materials Science Division, Lawrence Berkeley National Laboratory, Berkeley, California 94720-3220, USA

[c]Johannes Gutenberg-Universitat Mainz, 55128 Mainz, Germany

[d]Helmholtz-Institut Mainz, GSI Helmholtzzentrum für Schwerionenforschung GmbH, 55128 Mainz, Germany

[e]Department of Physics, University of California – Berkeley, Berkeley, California 94720, USA

KEYWORDS: zero- to ultra-low-field nuclear magnetic resonance (ZULF NMR); *J*-spectroscopy; quadrupolar nuclei; spin-spin interactions; optically pumped magnetometers.

*Corresponding author: dbarskiy@uni-mainz.de (Danila A. Barskiy)

ABSTRACT

Zero- to ultralow-field (ZULF) nuclear magnetic resonance (NMR) is a powerful version of NMR that allows studying molecules and their transformations in the regime dominated by intrinsic spin-spin interactions. While spin dynamics at zero magnetic field can be probed indirectly—via shuttling the sample that underwent evolution at zero field to a high-field NMR spectrometer for detection—*J*-spectra can also be measured directly at zero field by using non-inductive sensors, for example, optically-pumped magnetometers (OPMs). A *J*-spectrum can be detected when a molecule contains at least two different types of magnetic nuclei (i.e., nuclei with different gyromagnetic ratios) that are coupled via *J*-coupling. Up to date, no pure *J*-spectra of molecules featuring the coupling to quadrupolar nuclei were reported. Here we show that zero-field *J*-spectra can be collected from molecules containing quadrupolar nuclei with $I = 1$ and demonstrate this for solutions containing various isotopologues of ammonium cations, namely, $^{14}NH_4^+$ and $^{15}ND_xH_{4-x}^+$ (where $x = 0$, 1, 2, or 3). Lower ZULF NMR signals are observed for molecules containing larger numbers of deuterons compared to protons; this is attributed to less overall magnetization and not to the scalar relaxation of the second kind. We analyze the energy structure and allowed transitions for the studied molecular cations in detail using perturbation theory and demonstrate that in the studied systems, different lines in *J*-spectra have different dependences on the magnetic pulse length allowing for unique on-demand zero-field spectral editing. Precise values for the ^{15}N-^{1}H, ^{14}N-^{1}H, and D-^{1}H coupling constants are extracted from the spectra and the difference in the reduced coupling constants is explained by the secondary isotope effect. Simple symmetric cations such as ammonium do not require expensive isotopic labeling for the observation of *J*-spectra and, thus, may expand applicability of ZULF NMR spectroscopy in biomedicine and energy storage.

1. Introduction

Zero- to ultralow-field nuclear magnetic resonance (ZULF NMR) is a variant of NMR in which measurements are performed in the absence of a large external magnetic field.[1-2] In such a regime (as opposed to conventional high-field NMR), intrinsic spin-spin interactions—*J*-couplings and dipole-dipole couplings—are not truncated by the coupling to the external magnetic field.[3-5] This condition opens a way for obtaining unique chemical information with modest instrumentation costs.[6-7] Because of its ability to detect subtle intrinsic spin-spin interactions that provide valuable information about chemical composition of the sample under study, ZULF NMR can serve as an advantageous detection modality in situations where the use of expensive superconducting magnets is not desirable or impossible.[8] In particular, the analysis of biologically-relevant samples (e.g., natural extracts or metabolites in bioreactors) using portable ZULF NMR sensors is a desirable goal.[9-10] In addition, applications of ZULF NMR include the search for axion-like dark matter and tabletop studies of the physics beyond the standard model.[11]

A typical ZULF NMR experiment consists of the following steps: (i) pre-polarizing a sample in an external magnetic field, (ii) shuttling of the sample to the zero-magnetic-field region, (iii) applying magnetic field pulse(s) to the sample (or fast, non-adiabatic switching off of the guiding magnetic field) to generate a coherent nuclear spin evolution at zero field, and (iv) acquiring the NMR signal using a sensitive (5-10 $fT/Hz^{1/2}$) optically-pumped magnetometer (OPM).[5-6] Processing of the signal in the form of free decay is performed in a manner similar to the high-field NMR experiments (i.e., via Fourier transformation).[12]

The first ZULF NMR measurements were performed on a handful of simple molecules containing a small number (2-5) of *J*-coupled nuclear spins. It was noted that in some cases ZULF NMR measurements did not result in observable *J*-spectra for substances under study.[13] Systems

that do not produce observable ZULF NMR spectra typically contain spin-1 nuclei, such as deuterium (D), ^{14}N, or ^{35}Cl.[14-16] These nuclei are quadrupolar since, besides having a magnetic dipole moment, they possess electric quadrupole moment and, therefore, interact with the electric field gradients. For this reason, quadrupolar coupling typically dominates other nuclear spin interactions and causes, in the presence of molecular tumbling, fast relaxation on the order of few milliseconds (compared to seconds for spin-1/2 nuclei) leading to broadening of the ZULF NMR lines.[12, 17-18]

In this work, we systematically study the effect of quadrupolar nuclei on the observable ZULF NMR *J*-spectra. As a system for such study, we have chosen aqueous solutions of ammonium cations prepared in mixtures of H_2O and D_2O at high acidity (concentration of H_2SO_4 and/or HCl is ~1M). We first demonstrate a *J*-spectrum of [^{14}N]-ammonium ($^{14}NH_4^+$) by taking advantage of the unique tetrahedral environment of the hydrogen atoms which effectively switches off quadrupolar interactions of the ^{14}N nucleus, see **Figure 1**. Expensive isotopic labeling is not required for the preparation of $^{14}NH_4^+$ extending application opportunities for symmetric molecular ions in zero-field *J*-spectroscopy. We then study the effect of deuterium in ZULF NMR spectra by detecting *J*-spectra of $^{15}ND_xH_{4-x}^+$ (where x = 0, 1, 2, or 3). Mixtures of $^{15}ND_xH_{4-x}^+$ were prepared by dissolving $^{15}NH_4Cl$ in solutions with varying D_2O/H_2O ratios and relying on rapid equilibration of isotopologues' concentrations due to chemical exchange between H^+/D^+ atoms.[9]

As part of the study of $^{15}ND_xH_{4-x}^+$ ions in ZULF NMR *J*-spectra, we show that due to the hierarchy of nuclear spin-spin interactions, different spectral lines in the *J*-spectra have different pulse-length dependences as demonstrated in experiment, rationalized by using perturbation theory, and confirmed by numerical simulations. We extract ^{15}N-^{1}H, ^{14}N-^{1}H spin-spin coupling values directly from *J*-spectra and notice the secondary isotope effect manifested as the difference

in the reduced coupling constants across ^{15}N-^{1}H and ^{14}N-^{1}H bonds. The value for the D-^{1}H scalar coupling in $^{15}NDH_3^+$ is extracted from the experiment in which various spectral lines in *J*-spectrum respond differently to the magnetic field excitation pulses. We additionally discuss possibility of creating and storing nuclear spin order in spin states with extended lifetime which in principle should be achievable in the symmetric molecular cations presented in this work. Since expensive isotopic labeling is not necessary for the observation of *J*-spectra, ZULF NMR spectroscopy of ammonium cations can be applied for probing materials relevant in biology and energy storage.

2. Results and Discussion

Zero-field *J*-spectra of ^{14}N- and ^{15}N-ammonium isotopologues. To understand general features of *J*-spectra at zero field, we start from the analysis of the ZULF NMR spectrum of [^{15}N]-ammonium, a molecular ion that does not contain quadrupolar nuclei. A *J*-spectrum of [^{15}N]-ammonium ion consists of two lines, one at 110.15 Hz and another at 183.58 Hz provided by the heteronuclear spin-spin (*J*-)coupling between ^{15}N and ^{1}H spins (**Figure 1A**). Particularly, the line at 110.45 Hz corresponds to $(3/2)|J_{15N\text{-}1H}|$, where $J_{15N\text{-}1H}$ = -73.43 Hz is the *J*-coupling between ^{15}N and ^{1}H nuclei and it arises from the transitions between nuclear-spin energy levels with the total proton spin $K_A = 1$ (**Figure 1B**). The line at 183.58 Hz corresponds to $(5/2)|J_{15N\text{-}1H}|$ and arises from the transitions between states with a total proton spin $K_A = 2$ (see Appendix for the detailed energy level analysis). A corresponding high-field ^{15}N NMR spectrum of the same sample would consist of five lines with intensities in the ratio of 1:4:6:4:1 separated by $J_{15N\text{-}1H}$ as expected from the binomial distribution for the projections of the total proton spin on the magnetic field axis.

In contrast, ZULF NMR spectrum of [^{14}N]-ammonium ion exhibits three well-resolved lines at 52.41 Hz, 104.82 Hz, and 157.23 Hz (**Figure 1A**). To explain this observation, one needs to consider five transitions, one in the $K_A = 0$ manifold, two in the $K_A = 1$ manifold, and two in the $K_A = 2$ manifold (**Figure 1C**). Two pairs of transitions overlap resulting in three distinct peaks at $J_{14N\text{-}1H}$, $2J_{14N\text{-}1H}$ and $3J_{14N\text{-}1H}$ in the ZULF NMR spectrum of $^{14}NH_4^+$ ($J_{14N\text{-}1H}$ = 52.41 Hz).

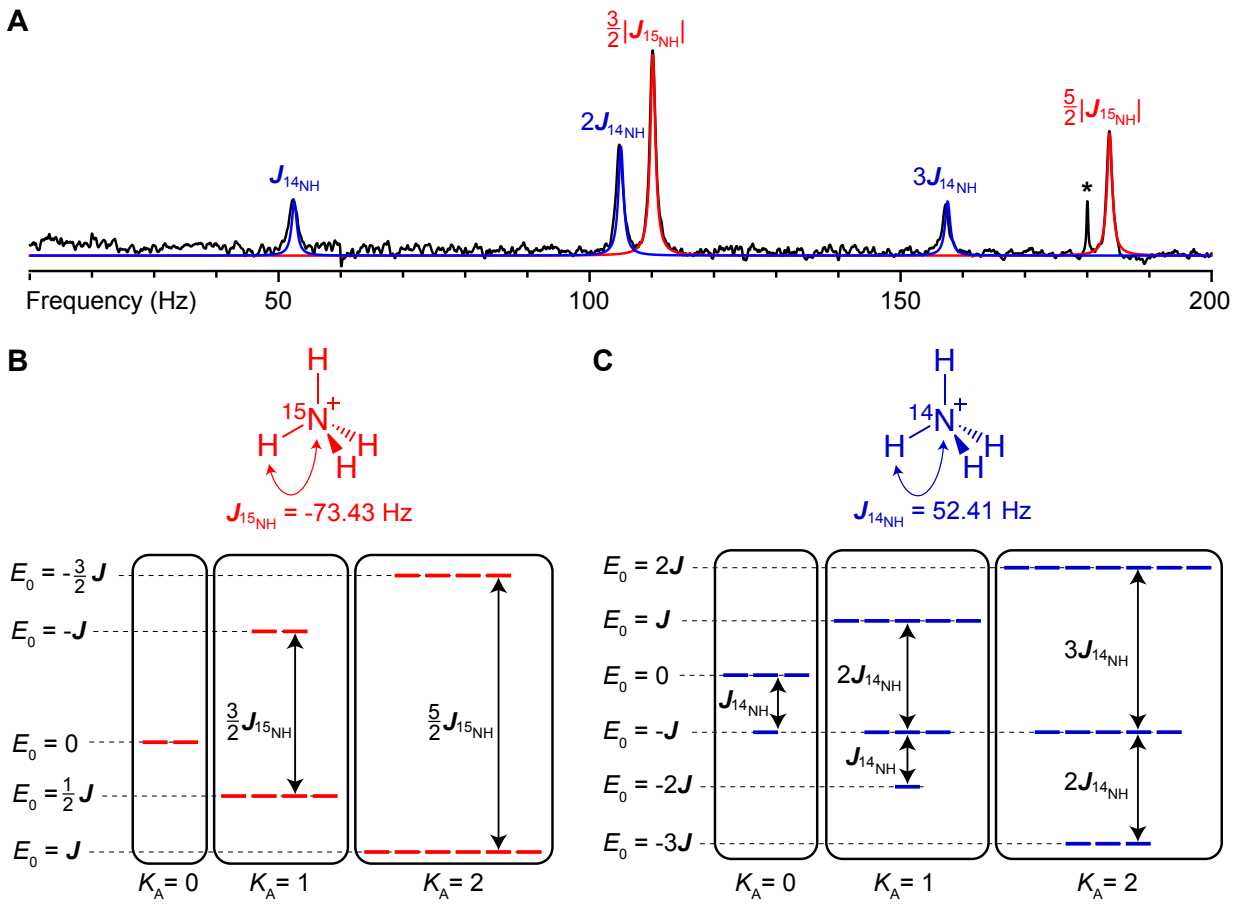

Figure 1. A) Zero-field NMR *J*-spectra of the mixture of [^{15}N]- and [^{14}N]-ammonium cations ($^{15}NH_4^+$ and $^{14}NH_4^+$) in aqueous solution of H_2SO_4 (1M). Asterisk depicts the third harmonic of the 60 Hz line frequency. B-C) Molecular diagram and nuclear spin energy-level structure of the [^{15}N]-ammonium and [^{14}N]-ammonium cation, respectively. Observable transitions correspond to spin flips in the manifolds conserving the total proton spin 0, 1, and 2. The main interaction in the system is heteronuclear *J*-coupling.

The mere fact of observing zero-field NMR *J*-spectrum of [^{14}N]-ammonium may seem surprising since ^{14}N is quadrupolar. Indeed, a typical nuclear spin Hamiltonian of the molecule containing quadrupolar nuclei is expected to have a large contribution arising from the interaction of the nuclear quadrupole moment with the electric field gradient created by the electrons at the site of the nucleus. For this reason, quadrupolar nuclei typically exhibit fast relaxation on

timescales of the order of a few milliseconds leading to their "self-decoupling". However, in the case of $^{14}NH_4^+$ cations, the ^{14}N is not self-decoupled because of the high symmetry of the molecule. In general, when quadrupolar nuclei are positioned at the center of a tetrahedral or an octahedral molecule, quadrupolar interaction is effectively switched off since electric field gradients are absent in such symmetric environments. For the same reason, the quadrupolar tensor is typically averaged out in isotropic liquids as a result of fast molecular motion.[18] Therefore, in the context of zero-field NMR, this allows us to treat ^{14}N in $^{14}NH_4^+$ and, as discussed below, D in $^{15}ND_xH_{4-x}^+$, as effectively non-quadrupolar nuclei with spin $I = 1$. However, it is important to note that in general, quadrupolar nuclei can still affect relaxation of the coupled nuclear spins and therefore can lead to broadening of spectral lines in ZULF NMR spectra. A T_1 measurement performed by varying the sample polarization time between 5 and 40 s indeed yielded slightly different T_1 values, i.e., $T_1(^{14}NH_4^+) = 12.5\pm0.2$ s compared to $T_1(^{15}NH_4^+) = 15.5\pm0.2$ s.[19]

Isotope Effects. The main difference in the experimentally observed $^{14}N-H$ and $^{15}N-H$ *J*-coupling constants is due to the primary isotope effect, i.e., the fact that the coupling strength between two nuclei is proportional to the product of the corresponding gyromagnetic ratios. However, even after the correction for gyromagnetic ratios, the difference in the reduced couplings is still noticeable (**Table A1**). For example, from multiple measurements of the NH_4Cl sample containing 60:40 mixture of ^{15}N and ^{14}N isotopes, the ratio of the *J*-couplings was determined as $\left|J_{^{15}NH}/J_{^{14}NH}\right| = 1.4012(2)$, as compared to table data for gyromagnetic ratios $\left|\gamma_{^{15}N}/\gamma_{^{14}N}\right| = 1.4027548(5)$.[20] Although small, this difference is an order of magnitude larger than experimental uncertainty and is a manifestation of the secondary isotope effect, i.e., changes in the electronic structure of molecules that affect Ramsey terms.[21] One should note that the main contribution to ^1H-($^{15}N/^{14}N$) *J*-coupling arises from the Fermi contact interaction and thus, spin-spin coupling

constant is positive for nuclei connected through one chemical bond in the case of positive gyromagnetic ratios.[22] Since ^{15}N and ^{14}N have different signs of gyromagnetic ratios, $^{15}NH_4^+$ and $^{14}NH_4^+$ have different signs of heteronuclear *J*-couplings as indicated by inverted structures of their nuclear spin energy levels (**Figure 1B,C**).

The fact that ammonium cations have several peaks in zero-field spectra (which are exact integer- or half-integer multiples of *J*) allows to extract *J*-coupling values in a more precise way by fitting experimental data with fewer parameters. Precision studies of *J*-couplings using zero-field NMR spectroscopy is a promising way to probe molecular chirality[23] and investigate parity non-conserving interactions in molecules[24]. In addition, precision measurements of molecular *J*-couplings in solution would allow comparing the results of calculating the precise molecular bond lengths by the tools of quantum chemistry with experiments, thus, making ZULF NMR a tool for benchmarking precision of quantum chemistry calculations.[25-26] Further analysis could explain the exact dependence of *J*-couplings in ammonia on the bond length (rotational and vibrational structure analysis) but we point out that the presented measurements are relatively simple and the investigated molecules are studied in liquid state and at the same container, thus, the effect of the dielectric properties of the environment and temperature are accounted equally for both cations.

Deuterium Isotopologues. To analyze the effect on *J*-spectra of a quadrupolar nucleus other than ^{14}N, we performed ZULF NMR measurements of different isotopologues of $^{15}ND_xH_{4-x}^+$ (where x = 0, 1, 2, or 3). While deuterium has spin I = 1 and is quadrupolar, its quadrupole moment is significantly smaller ($0.29 \cdot 10^{-30}$ m^2) than that of ^{14}N ($1.56 \cdot 10^{-30}$ m^2)[18] and therefore, its effect on ZULF NMR spectra is expected to be less pronounced. This expectation is now confirmed by the experiment as discussed below.

To prepare $^{15}ND_xH_{4-x}^+$ samples, the amount of deuterium was controlled by varying the ratio of H_2O/D_2O in the solution. Here and below, we refer to isotopologues as xD where x represents a number of D atoms in the molecule. Since chemical exchange leads to equilibration of various ammonium-isotopologue concentrations, a molar fraction χ of the isotopologue xD can be derived from the fraction p of the deuterium in solution as

$$\chi = \binom{4}{x} p^x (1-p)^{4-x}. \quad (1)$$

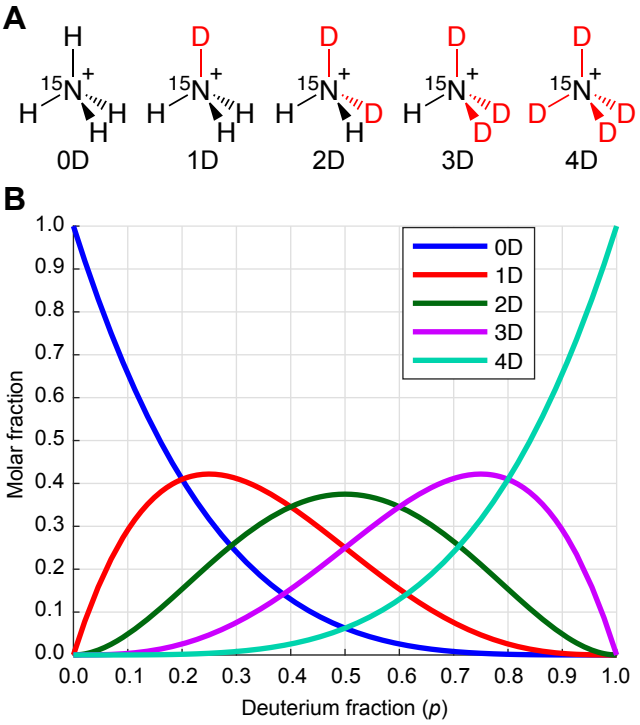

Figure 2. A) Isotopologues of the ammonium cation ($^{15}ND_xH_{4-x}^+$) are present in the aqueous solution. The fraction of deuterium (D) was varied by changing the amount of H_2O vs. D_2O. Isotopologues are labeled xD where x represents a number of D atoms in the molecule. B) Equilibrium molar fractions of the isotopologues as a function of deuterium fraction in solution as determined by eq. (1).

Figure 3 compares zero-field NMR spectra with high-field (18.8 T) ^{15}N NMR spectra of samples containing ammonium chloride prepared by varying p, a fraction of deuterium in solution. It is well known that ammonium ions undergo reversible hydrogen exchange with water.[27] High acidity of the samples can slow down the hydrogen exchange rate from ≈50,000 s^{-1} down to ≈2 s^{-1}, thus, allowing for the molecule to exist long enough for exhibiting nuclear spin coherences that can be detected by ZULF NMR spectroscopy.[9]

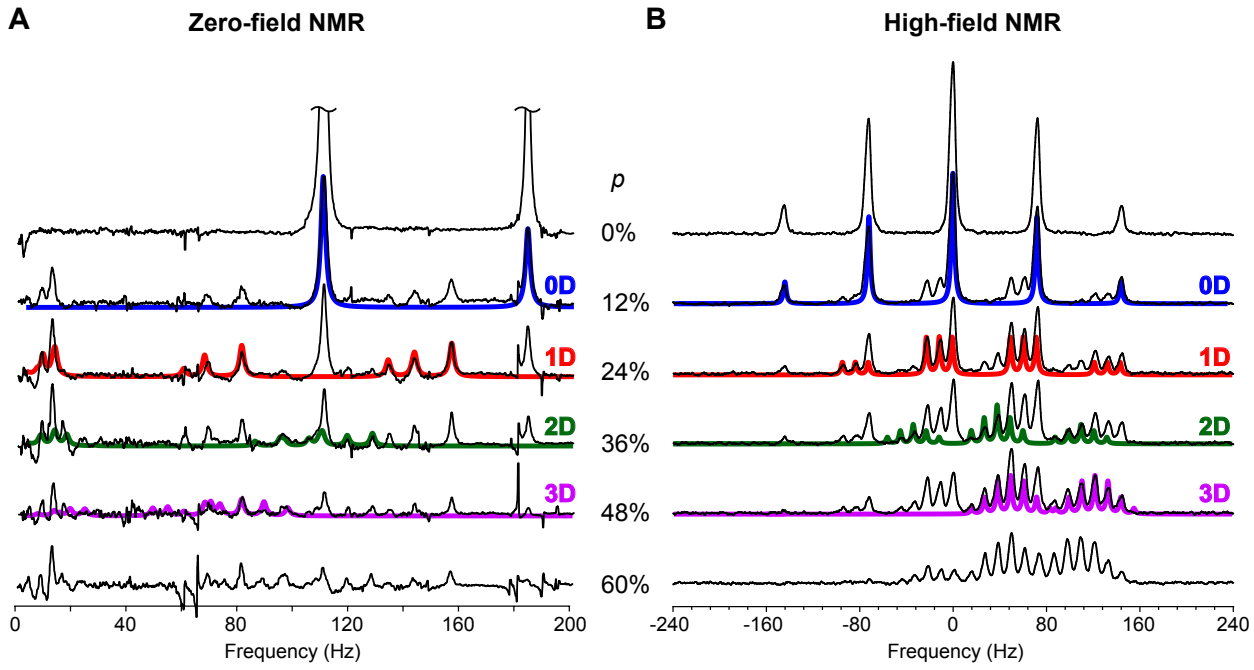

Figure 3. Experimentally measured (A) zero-field NMR spectra and (B) high-field (16.8 T) ^{15}N NMR spectra of solutions containing a mixture of isotopologues of ammonium, $^{15}ND_xH_{4-x}^+$, prepared by varying the molar fraction of deuterium, p, in aqueous solutions. Simulated NMR spectra for the individual isotopologues 0D, 1D, 2D and 3D are overlaid (where xD represents the number x of deuterium atoms in the molecule).

Upon increase of the deuterium fraction (p), spectroscopic signatures of $^{15}NH_4^+$ gradually decrease; this is evident from both zero-field and high-field NMR spectra (**Figure 3A-B**).

However, these spectroscopic changes are more evident in ZULF NMR spectra because the elimination of chemical shift simplifies analysis of the spectra. While each of the chemicals has its own spectroscopic signatures characterized by a unique set of frequencies in *J*-spectra (**Figure 3A**), high-field ^{15}N NMR spectra of isotopologues suffer from the overlap of different multiplets and changes of the ^{15}N chemical shift, due to the changes in electronic density on the nitrogen atom upon increasing a number of deuterium atoms, *x*, from 0 to 4 (**Figure 3B**).

The main reason of the decreased ZULF NMR signal for ammonium cations with larger deuterium content is smaller initial magnetization of the sample due to decreased number of protons. Indeed, in a simple two-spin case, ZULF NMR signal is proportional to the difference between gyromagnetic ratios of the *J*-coupled nuclei.[5] In case of many-spin systems composed of more than two types of heteronuclei, the detected signal depends on a combination of gyromagnetic ratios determined by the exact nuclear spin topology of the molecule.[28] However, the general trend is that the main magnetization-contributing nuclei, protons, predominantly contribute to the observed signal as they have significantly larger gyromagnetic ratio compared to other spins in the system, for example, $\gamma_{^1\mathrm{H}}/\gamma_{^{15}\mathrm{N}} \approx -10$ and $\gamma_{^1\mathrm{H}}/\gamma_{^2\mathrm{H}} \approx 6.5$.

The fact that the signal intensity in the *J*-spectrum of the molecule depends not only on the concentration but also on the exact spin-type composition and spin topology presents a general limitation of ZULF NMR spectroscopy for chemical analysis. This is in contrast to the case of conventional high-field NMR where the detected signal is proportional to molecular concentration independent of topology. Therefore, for analytical purposes, ZULF NMR spectral features of different chemicals should be calibrated (or simulated) for direct spectroscopic comparison. The agreement between the experimentally obtained and the simulated ZULF NMR spectra is excellent for the molecules $^{15}NH_4^+$, $^{15}NDH_3^+$, and $^{15}ND_2H_2^+$ (**Figure 3**). Signatures of other isotopologues

$^{15}ND_xH_{4-x}^+$ (where x is 3 and 4) are noticeable in the spectra as well, however, their signal is significantly lower and, therefore, spectroscopic assignment is less straightforward.

We note that another possible reason of the decreased NMR signal for the molecules with larger deuterium content is scalar relaxation of the second kind (SR2K).[29] In the context of ultralow-field NMR, SR2K may lead to accelerated relaxation of overall polarization as well as coherences involving spin-½ nuclei mediated through the *J*-couplings with the quadrupolar nucleus in the regime where nuclei are strongly coupled. In other words, when spins are strongly coupled, they tend to relax together rather than separately. For example, fast liquid-state polarization decay was observed for hyperpolarized [5-^{13}C]-glutamine during the transfer to an MRI scanner when the transfer field was below 800 μT and was attributed to the SR2K caused by the fast-relaxing quadrupolar ^{14}N-nucleus adjacent to the ^{13}C nucleus in the amide group.[30] Another recent study showed that partially deuterated ethanols have significantly larger linewidth in near-zero-field Larmor-precession experiments implying a strong SR2K contribution to ^{1}H relaxation rates despite relatively weak coupling constants on the order of 1-2 Hz.[14]

It is clear, however, that the situation is completely different for $^{15}ND_xH_{4-x}^+$ isotopologues investigated in our work because, first, we do observe their *J*-spectra and second, the linewidth of resonances is determined by the intermolecular chemical exchange and not SR2K mechanism. The absence of an overwhelming SR2K contribution may potentially be explained by the fact that the quadrupolar relaxation rates of the spin state imbalances in $^{15}ND_xH_{4-x}^+$ are determined by the correlation time of the molecular rotations and thus, symmetry properties of these molecules have to be accounted for. An exact explanation of the relaxation phenomena at zero field requires additional analysis which lies beyond the scope of this paper. We note that similar effects, i.e.,

long-lived spin states in molecules containing deuterium, were demonstrated for the deuterated methyl groups.[31]

As a general rule of thumb, *J*-spectra featuring couplings to quadrupolar nuclei should be observable at ZULF conditions if the corresponding *J*-coupling is manifested in conventional high-field NMR spectra. For example, in the **Figure 3B**, a splitting to D atoms is clearly observed in ^{15}N NMR spectra.

Pulse-length dependence. High-field ^{1}H NMR measurements cannot directly resolve ^{1}H-D *J*-coupling in $^{15}ND_xH_{4-x}^{+}$ systems. For example, **Figure 4A** shows a ^{1}H NMR spectrum of the ammonium solution with 24% fraction of deuterium atoms. One can clearly see a series of doublets split by heteronuclear ^{1}H-^{15}N *J*-coupling of -73.4 Hz shifted to lower field for each isotopologue $^{15}ND_xH_{4-x}^{+}$ as x increases from 0 to 2, however, the fine structure corresponding to ^{1}H-D coupling is not visible and only broadening of the peaks is observed. To investigate opportunities of resolving ^{1}H-D *J*-coupling with zero-field NMR techniques, we simulated the zero-field spectra for deuterated ammonium isotopologues and analyzed their energy level structures using the perturbation theory (see Appendix).

For all isotopologues $^{15}ND_xH_{4-x}^{+}$ (where $x = 1 - 3$) one can distinguish regions of low- and high-frequency peaks (e.g., **Figure 4B**). High-frequency peaks correspond to transitions within the strongly-coupled subsystem consisting of ^{15}N and ^{1}H spins when total deuterium spin remains unchanged. Low-frequency peaks correspond to the deuterium spin flips keeping the strongly-coupled ^{15}N-^{1}H subsystem unperturbed. These groups of peaks are expected to respond differently to the magnetic pulse excitation and thus, by plotting their integrals as a function of magnetic pulse length, one can extract information about subtle spin-spin interactions which otherwise would have taken more sophisticated multinuclear high-field NMR analysis.

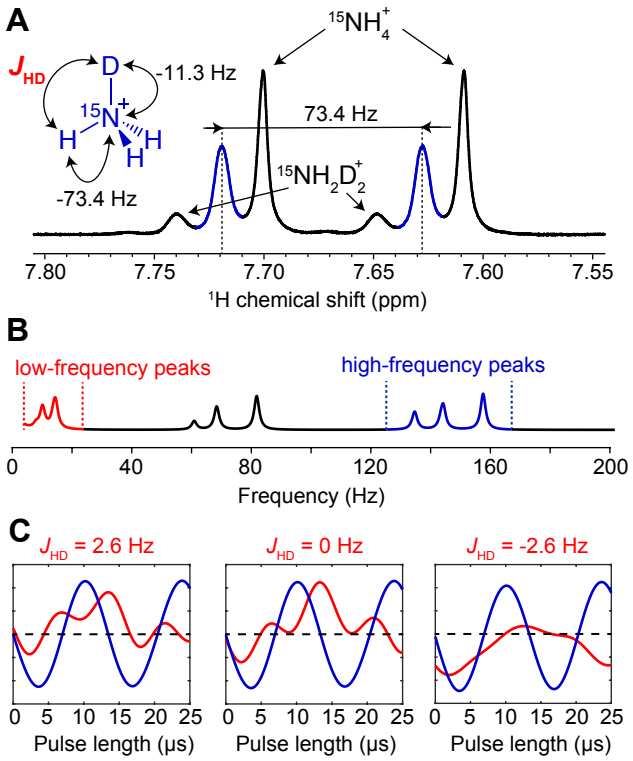

Figure 4. A) ^{1}H NMR spectrum of $^{15}ND_xH_{4-x}^+$ solution with deuterium fraction p = 24%. B) Calculated zero-field J-spectrum of $^{15}NDH_3^+$ featuring low-frequency (0-15 Hz, red) and high-frequency (120-180 Hz, blue) region of the spectrum. C) Calculated integrals for the low-frequency (0-15 Hz, red) and high-frequency (120-180 Hz, blue) peaks in the spectrum of $^{15}NDH_3^+$ as a function of the magnetic pulse excitation length.

For example, for $^{15}NDH_3^+$ one can clearly see that different ^{1}H-D J-couplings result in different calculated dependencies of low-frequency integrals on the excitation pulse length (**Figure 4C**). Even a subtle change of ~3 Hz dramatically modifies the pulse length dependence. Importantly, not only a magnitude but also a sign of the J-coupling can be understood by experimentally probing the pulse-length dependence.

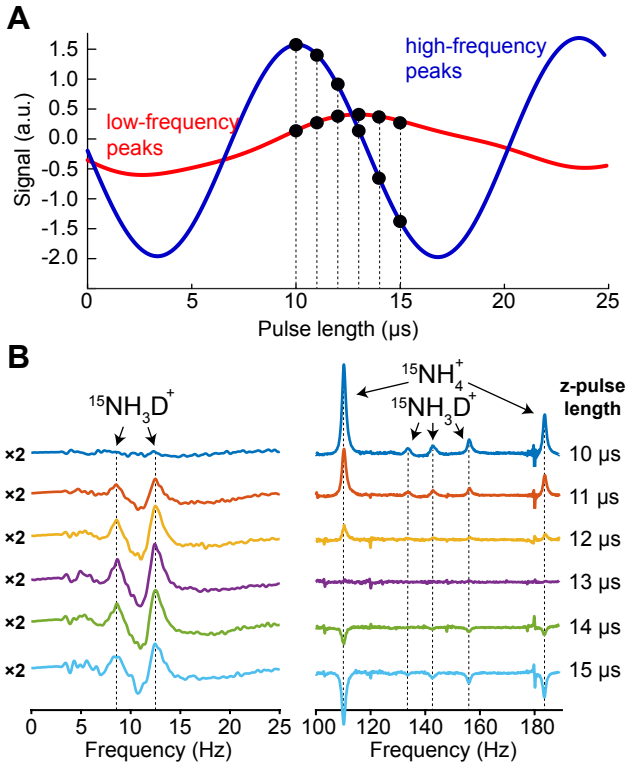

Figure 5. A) Theoretical calculation of the ZULF NMR signal amplitude for the low- and high-frequency spectral regions of $^{15}NDH_3^+$ (same as the last graph in Figure 4C). B) ZULF NMR spectra of $^{15}ND_xH_{4-x}^+$ solution with deuterium fraction $p = 24\%$ recorded after the action of constant-amplitude magnetic field pulses with various duration (10-15 μs, amplitude 1.6 mT) applied in a direction of the magnetometer-detection axis. Note that the low-frequency (0-15 Hz) and high-frequency (100-200 Hz) parts of the spectrum respond differently to the magnetic pulse excitation.

This is indeed observed in the experiment. For $^{15}NDH_3^+$ assuming *J*-coupling of -2.6 Hz, both calculations and experiments demonstrate that high-frequency peaks have maximal intensity for the pulse length of ≈10 μs (field amplitude is 1.6 mT) while low-frequency signals are negligible at this pulse duration (**Figure 5**). For the same molecule, the pulse length of 13 μs maximizes low-frequency peaks while making high-frequency peaks vanish. This ability to

maximize some parts of the *J*-spectra while suppressing others opens possibilities for on-demand spectral editing in zero-field NMR spectroscopy. Indeed, in case when complex chemical mixtures are studied using ZULF NMR tools, this feature could yield an additional degree of freedom for disentangling the spectral complexity. In principle, this experiment can be performed in a two-dimensional (2D) manner where Fourier transformation in the indirect (pulse length) dimension would give separate peaks in the 2D spectrum revealing additional information about spin topology that may simplify molecular characterization.

3. Conclusions and Outlook

Symmetric ions such as $^{14}NH_4^+$ and $^{15}NH_4^+$ (**Figure 1**, insert) represent an interesting class of molecules that may possess nuclear spin orders with extended lifetimes. Indeed, less symmetric analogs of ammonium, methyl groups, are known to support long-lived spin states (LLSS)[32-33] and long-lived coherences (LLC)[34] due to the fact that transitions between states of different irreducible representations are symmetry-forbidden for dipole-dipole relaxation.[31] While LLSS have already been observed in $^{13}CH_3/^{13}CD_3$ groups,[31, 35-36] the search of LLSS in $^{14}NH_4^+/^{15}NH_4^+$ is certainly warranted. The ability to store nuclear spin coherences for a long time will enable enhanced spectral resolution (i.e., narrow lines) in zero-field NMR. In addition, the existence of the LLSS in symmetric ions could allow preserving hyperpolarization on the timescale significantly longer than T_1. One should note that hyperpolarization of ammonia and its derivatives was recently demonstrated by using signal amplification by reversible exchange (SABRE) approach.[37-38]

Biologically relevant molecules containing nitrogen atoms in low-symmetry tetrahedral environments may also be an object for future investigation by the ZULF NMR research

community. For example, choline and its derivates are proposed as biomarkers for cancer diagnosis and response to treatment using hyperpolarized *in vivo* NMR spectroscopy.[39-40] While most of the research to date is focused on polarizing ^{15}N-labeled choline derivatives, preparation of hyperpolarized ^{14}N magnetization in non-labeled (i.e., ^{14}N-containing) molecules is feasible as well. While T_1 of ^{14}N sites in choline is still relatively short (~4 s),[41] which may limit applicability of the conventional approach, the long-lived spin states can provide a platform for the storage of enhanced population imbalance. At the same time, ZULF NMR detection of the characteristic spectroscopic signatures does not require hyperpolarization and therefore, small molecules containing ^{14}N in semi-symmetric environments can be used as tracers for *in vivo* ZULF NMR studies. For example, acetylcholine is an important neurotransmitter and its monitoring by optical magnetometers could yield invaluable metabolic information.[42] Feasibility for the realization of these ideas is supported by the fact that ^{1}H–^{14}N heteronuclear correlation (HSQC) spectroscopy of choline-containing compounds in solutions has been successfully demonstrated *in vitro*[41] and *in vivo* (*i.e.*, "rule of thumb" for quadrupolar nuclei is fulfilled).[43-44] In addition to biomedicine, zero-field *J*-spectroscopy of ammonium (and other symmetric ions) can also find application for probing Bronsted acid sites in zeolites, lipid bilayers, and the hydrated ionomer membranes such as Nafion used in fuel cells.[45]

To summarize, we reported zero-field NMR measurements of molecules featuring the *J*-coupling to quadrupolar nuclei. Solutions containing different isotopologues of ammonium cations, $^{14}NH_4^+$ and $^{15}ND_xH_{4-x}^+$ (where x = 0, 1, 2, or 3) were studied and their zero-field NMR *J*-spectra were measured. Molecules containing a larger number of deuterons compared to protons are characterized by a lower intensity of resonances in *J*-spectra as attributed to the decreased number of protons in the molecule (less overall magnetization) and not the scalar relaxation of the

second kind. For the spin systems containing more than two types of magnetic nuclei, different groups of peaks in *J*-spectra may have a different dependence of the magnetic pulse length provided a suitable hierarchy of nuclear spin-spin interactions. We demonstrate this for $^{15}NDH_3^+$ and extract the $J_{1H\text{-}D}$ = -2.6(1) Hz using unequal pulse-length dependence of its low- and high-frequency peaks. Precise values for the ^{15}N-^{1}H and ^{14}N-^{1}H coupling constants are extracted from the *J*-spectra of $^{15}NH_4^+$ and $^{14}NH_4^+$ and the difference in the reduced coupling constants is explained by the secondary isotope effect. Subtle differences in electronic structure for $^{15}NH_4^+$ and $^{14}NH_4^+$ are reported via measuring their *J*-couplings in the liquid phase. Isotopologues of ammonia can be conveniently detected by optical magnetometers at zero magnetic field providing chemical specificity without need for expensive isotopic labeling. These results pave the way for studying long-lived spin states in molecules containing quadrupolar nuclei and for applications of ZULF NMR in biomedicine and energy storage.

4. Methods

Zero-field NMR spectra of the ammonium samples were recorded in a home-built ZULF NMR spectrometer (incorporating ^{87}Rb atomic magnetometer inside multilayer magnetic shielding). Physical principles of operation, construction, and calibration of the instrument are described in detail in Ref. 6. Each zero-field spectrum is a result of 100 averages, polarization time is 30 s in the field of 2 T, shuttling time to the zero-field chamber is ~0.5 s. During the shuttling, no guiding field was applied. To generate an observable ZULF NMR signal, a magnetic pulse of variable length was applied in a direction of the magnetometer sensitive axis.

Solutions of $^{15}NH_4Cl$ (Sigma-Aldrich 299251) and/or $^{14}NH_4Cl$ (Sigma-Aldrich 254134) were prepared in a 6 M concentration by dissolving them in concentrated hydrochloric acid. Each sample (150 μL for ZULF NMR measurements and 600 μL for high-field NMR measurements) was pipetted into a standard 5 mm NMR tube and flame-sealed before the measurement. High-field ^{15}N NMR measurements were performed at room temperature using an 800 MHz (16.8 T) Bruker NMR spectrometer.

Solutions of $^{15}ND_xH_{4-x}^+$ were prepared by dissolving $^{15}NH_4Cl$ (94.6 mg per vial) into a mixture of distilled water and D_2O (Cambridge Isotope Laboratories DLM-4-99.8-1000) according to a desired deuterium fraction (p) followed by the addition of concentrated HCl (12.18 M) to yield a total volume of 0.3 mL. The solutions were transferred to standard 5 mm NMR tubes and subsequently sealed with a flame.

Zero-field spectra of $^{14}NH_4^+$ and $^{15}ND_xH_{4-x}^+$ were calculated in MATLAB using numerical diagonalization of the observable operator and the zero-field Hamiltonian. Additionally,

an analytical perturbation model was used (see Appendix) to cross-check numerical calculation and to gain better understanding of underlying physics in the studied molecular systems.

5. Appendix

Amongst all possible nuclear spin interactions, only electron-mediated *J*-couplings are important for analyzing the zero-field NMR spectra of molecules in the liquid state. The nuclear spin Hamiltonian ($\widehat{H}$) for different isotopologues of the ammonium cation ($^{15}ND_xH_{4-x}^{+}$, where x can take values from 0 to 4) is therefore given by

$$\widehat{H} = J_{\mathrm{NH}}\left(\hat{\mathbf{S}} \cdot \widehat{\mathbf{K}}_{\mathrm{A}}\right) + J_{\mathrm{ND}}\left(\hat{\mathbf{S}} \cdot \widehat{\mathbf{K}}_{\mathrm{B}}\right) + J_{\mathrm{HD}}\left(\widehat{\mathbf{K}}_{\mathrm{A}} \cdot \widehat{\mathbf{K}}_{\mathrm{B}}\right), \tag{A1}$$

where we follow the notation suggested by Butler et al.,[28] i.e., $\hat{\mathbf{S}}$ denotes the spin of the heteronucleus (in our case, ^{15}N), $\widehat{\mathbf{K}}_{\mathrm{A}}$ denotes the total proton spin ($\widehat{\mathbf{K}}_{\mathrm{A}} = \sum_{i=1}^{4-x} \hat{\mathbf{I}}_i^{\mathrm{H}}$), and $\widehat{\mathbf{K}}_{\mathrm{B}}$ denotes the total deuterium spin ($\widehat{\mathbf{K}}_{\mathrm{B}} = \sum_{i=1}^{x} \hat{\mathbf{I}}_i^{\mathrm{D}}$). The values of the couplings were extracted from the experimentally measured spectra and are shown in the **Table A1**. Notice that due to the electronic similarity of ^{1}H and D, the coupling between ^{15}N and D can be estimated as $J_{\mathrm{ND}} \approx J_{\mathrm{NH}}\left(\frac{\gamma_{\mathrm{D}}}{\gamma_{\mathrm{H}}}\right)$. Below we derive the zero-field NMR frequencies in *J*-spectra for different isotopologues of ammonium cation.

Table A1. Heteronuclear *J*-couplings in the $^{15}ND_xH_{4-x}^{+}$ and $^{14}NH_4^{+}$ spin systems measured in this work.

	Coupling value (Hz)
$J_{15\mathrm{NH}}$	-73.4291±0.0020*
$J_{14\mathrm{NH}}$	52.4064±0.0039*
$J_{15\mathrm{ND}}$	-11.3**
J_{HD}	-2.6*

*data extracted from zero-field NMR spectra

**data extracted from high-field (800 MHz) ^{15}N NMR spectra

A1. Analytical calculation of zero-field NMR spectrum of $^{15}NH_4^+$

For $x = 0$ eq. (A1) simplifies to

$$\hat{H} = J_{\mathrm{NH}}(\hat{\mathbf{S}} \cdot \hat{\mathbf{K}}_{\mathrm{A}}). \tag{A2}$$

By introducing the total spin ($\hat{\mathbf{F}}_{\mathrm{A}}$) of the ^{15}N-^{1}H system as $\hat{\mathbf{F}}_{\mathrm{A}} = \hat{\mathbf{S}} + \hat{\mathbf{K}}_{\mathrm{A}}$, one can show that

$$\hat{\mathbf{S}} \cdot \hat{\mathbf{K}}_{\mathrm{A}} = \frac{1}{2}\left(\hat{\mathbf{F}}_{\mathrm{A}}^2 - \hat{\mathbf{S}}^{\mathbf{2}} - \hat{\mathbf{K}}_{\mathrm{A}}^2\right). \tag{A3}$$

Thus, eigenstates of the Hamiltonian (A2) denoted $|F_{\mathrm{A}}, K_{\mathrm{A}}\rangle$, can be expressed using quantum numbers F_{A} and K_{A} (corresponding to the operators $\hat{\mathbf{F}}_{\mathrm{A}}^2$ and $\hat{\mathbf{K}}_{\mathrm{A}}^2$) and their energies ($E$) can be determined using the equation

$$E = \frac{J_{\mathrm{NH}}}{2}\left(F_{\mathrm{A}}(F_{\mathrm{A}}+1) - S(S+1) - K_{\mathrm{A}}(K_{\mathrm{A}}+1)\right). \tag{A4}$$

Since $\hat{\mathbf{K}}_{\mathrm{A}}^2$ and $\hat{\mathbf{S}}^{\mathbf{2}}$ commute with the perturbation (magnetic DC pulse along z-direction), transitions between eigenstates are constrained by $\Delta K_{\mathrm{A}} = \Delta S = 0$, while $\Delta F_{\mathrm{A}} = 0, \pm 1$. Therefore, for $^{15}NH_4^+$ we expect peaks at $\frac{5}{2}J_{\mathrm{NH}}$ and $\frac{3}{2}J_{\mathrm{NH}}$, corresponding to transitions between $\left|\frac{5}{2}, 2\right\rangle \rightarrow \left|\frac{3}{2}, 2\right\rangle$ and $\left|\frac{3}{2}, 1\right\rangle \rightarrow \left|\frac{1}{2}, 1\right\rangle$ as shown in the **Table A2**.

Table A2. Nuclear spin eigenstates, corresponding energies, allowed transitions and zero-field NMR spectral frequencies of $^{15}NH_4^+$ ion.

Eigenstate, $\lvert F_{\mathrm{A}}, K_{\mathrm{A}}\rangle$	Energy	Transition	Spectral frequency
$\left\lvert\frac{5}{2}, 2\right\rangle$	J_{NH}	$\left\lvert\frac{5}{2}, 2\right\rangle \rightarrow \left\lvert\frac{3}{2}, 2\right\rangle$	$\frac{5}{2}J_{\mathrm{NH}}$

$\left\|\frac{3}{2},2\right\rangle$	$-\frac{3}{2}J_{\mathrm{NH}}$	$\left\|\frac{3}{2},1\right\rangle \rightarrow \left\|\frac{1}{2},1\right\rangle$	$\frac{3}{2}J_{\mathrm{NH}}$
$\left\|\frac{3}{2},1\right\rangle$	$\frac{1}{2}J_{\mathrm{NH}}$		
$\left\|\frac{1}{2},1\right\rangle$	$-J_{\mathrm{NH}}$		
$\left\|\frac{1}{2},0\right\rangle$	0		

A2. Analytical calculation of zero-field NMR spectrum of $^{15}NDH_3^+$

Since $|J_{\mathrm{ND}}|, |J_{\mathrm{HD}}| < |J_{\mathrm{NH}}|$, we can apply perturbation theory and split the Hamiltonian (A1) into two parts:

$$\widehat{H} = \widehat{H}_0 + \widehat{H}_1, \tag{A5}$$

where $\widehat{H}_0 = J_{\mathrm{NH}}\left(\hat{\mathbf{S}} \cdot \widehat{\mathbf{K}}_{\mathrm{A}}\right)$ is the same as in eq. (A2) and $\widehat{H}_1 = J_{\mathrm{ND}}\left(\hat{\mathbf{S}} \cdot \widehat{\mathbf{K}}_{\mathrm{B}}\right) + J_{\mathrm{HD}}\left(\widehat{\mathbf{K}}_{\mathrm{A}} \cdot \widehat{\mathbf{K}}_{\mathrm{B}}\right)$. Hamiltonian $\widehat{H}_1$ can be simplified further. Using geometric arguments presented in the ref. 28, one may show that $\hat{\mathbf{S}}$ and $\widehat{\mathbf{K}}_{\mathrm{A}}$ can be replaced by their projections on $\hat{\mathbf{F}}_{\mathrm{A}}$:

$$\widehat{H}_1 = J_{\mathrm{ND}}\left(\hat{\mathbf{S}} \cdot \widehat{\mathbf{K}}_{\mathrm{B}}\right) + J_{\mathrm{HD}}\left(\widehat{\mathbf{K}}_{\mathrm{A}} \cdot \widehat{\mathbf{K}}_{\mathrm{B}}\right) = J_{\mathrm{ND}} \frac{\langle \hat{\mathbf{S}} \cdot \hat{\mathbf{F}}_{\mathrm{A}} \rangle}{\langle \hat{\mathbf{F}}_{\mathrm{A}}^2 \rangle}\left(\hat{\mathbf{F}}_{\mathrm{A}} \cdot \widehat{\mathbf{K}}_{\mathrm{B}}\right) + J_{\mathrm{HD}} \frac{\langle \widehat{\mathbf{K}}_{\mathrm{A}} \cdot \hat{\mathbf{F}}_{\mathrm{A}} \rangle}{\langle \hat{\mathbf{F}}_{\mathrm{A}}^2 \rangle}\left(\hat{\mathbf{F}}_{\mathrm{A}} \cdot \widehat{\mathbf{K}}_{\mathrm{B}}\right) =$$

$$= \frac{J_{\mathrm{ND}}^{\parallel} + J_{\mathrm{HD}}^{\parallel}}{2}\left(\hat{\mathbf{F}}^{\mathbf{2}} - \hat{\mathbf{F}}_{\mathrm{A}}^2 - \widehat{\mathbf{K}}_{\mathrm{B}}^2\right), \tag{A6}$$

where $\hat{\mathbf{F}} = \hat{\mathbf{F}}_{\mathrm{A}} + \widehat{\mathbf{K}}_{\mathrm{B}}$ is the total spin of the system. This notation suggests that there are no longer single couplings between protons and the heteronucleus to the deuterium atoms but rather a total coupling of the strongly coupled system $\left(\hat{\mathbf{S}}, \widehat{\mathbf{K}}_{\mathrm{A}}\right)$ to the weakly coupled deuterium $\left(\widehat{\mathbf{K}}_{\mathrm{B}}\right)$. Since $\widehat{\mathbf{K}}_{\mathrm{A}} = \hat{\mathbf{F}}_{\mathrm{A}} - \hat{\mathbf{S}}$ and $\hat{\mathbf{S}} = \hat{\mathbf{F}}_{\mathrm{A}} - \widehat{\mathbf{K}}_{\mathrm{A}}$, by analogy with (A3) one may find that

$$J_{\mathrm{ND}}^{\parallel} = J_{\mathrm{ND}} \frac{\langle \hat{\mathbf{S}} \cdot \hat{\mathbf{F}}_{\mathrm{A}} \rangle}{\langle \hat{\mathbf{F}}_{\mathrm{A}}^2 \rangle} = J_{\mathrm{ND}} \frac{\left(F_{\mathrm{A}}(F_{\mathrm{A}}+1)+S(S+1)-K_{\mathrm{A}}(K_{\mathrm{A}}+1)\right)}{2F_{\mathrm{A}}(F_{\mathrm{A}}+1)} \tag{A7}$$

and

$$J_{\mathrm{HD}}^{\parallel} = J_{\mathrm{HD}} \frac{\langle \hat{\mathbf{K}}_{\mathrm{A}} \cdot \hat{\mathbf{F}}_{\mathrm{A}} \rangle}{\langle \hat{\mathbf{F}}_{\mathrm{A}}^2 \rangle} = J_{\mathrm{HD}} \frac{\left(F_{\mathrm{A}}(F_{\mathrm{A}}+1)+K_{\mathrm{A}}(K_{\mathrm{A}}+1)-S(S+1)\right)}{2F_{\mathrm{A}}(F_{\mathrm{A}}+1)}. \tag{A8}$$

Since $K_{\mathrm{B}} = 1$, i.e., it is fixed, and we are left with F, F_{A}, and K_{A} as the quantum numbers for defining the eigenstates of $\widehat{H}$ which will be denoted as $|F, F_{\mathrm{A}}, K_{\mathrm{A}}\rangle$. **Table A3** shows eigenstates, allowed transitions and corresponding spectral lines. Note that we distinguish between high-frequency and low-frequency transitions. High-frequency transitions are transitions in which the quantum number of the strongly coupled system (F_{A}) changes. If $\Delta F_{\mathrm{A}} = 0$ and only F changes, we will refer to these transitions as low-frequency transitions. These transitions can therefore be seen as deuterium spin flip. The only allowed transitions are those that leave K_{A} unchanged.

Table A3. Nuclear spin eigenstates, corresponding energies, allowed transitions and zero-field NMR spectral frequencies of $^{15}NDH_3^+$ ion.

Eigenstate, $\lvert F, F_{\mathrm{A}}, K_{\mathrm{A}}\rangle$	E_0	E_1
$\left\lvert 3, 2, \frac{3}{2}\right\rangle$	$\frac{3}{4}J_{\mathrm{NH}}$	$\frac{1}{2}(J_{\mathrm{ND}} + 3J_{\mathrm{HD}})$
$\left\lvert 2, 2, \frac{3}{2}\right\rangle$	$\frac{3}{4}J_{\mathrm{NH}}$	$-\frac{1}{4}(J_{\mathrm{ND}} + 3J_{\mathrm{HD}})$
$\left\lvert 1, 2, \frac{3}{2}\right\rangle$	$\frac{3}{4}J_{\mathrm{NH}}$	$-\frac{3}{4}(J_{\mathrm{ND}} + 3J_{\mathrm{HD}})$
$\left\lvert 2, 1, \frac{3}{2}\right\rangle$	$-\frac{5}{4}J_{\mathrm{NH}}$	$\frac{1}{4}(-J_{\mathrm{ND}} + 5J_{\mathrm{HD}})$
$\left\lvert 1, 1, \frac{3}{2}\right\rangle$	$-\frac{5}{4}J_{\mathrm{NH}}$	$-\frac{1}{4}(-J_{\mathrm{ND}} + 5J_{\mathrm{HD}})$
$\left\lvert 0, 1, \frac{3}{2}\right\rangle$	$-\frac{5}{4}J_{\mathrm{NH}}$	$-\frac{1}{2}(-J_{\mathrm{ND}} + 5J_{\mathrm{HD}})$

$\left\|2,1,\frac{1}{2}\right\rangle$	$\frac{1}{4}J_{\mathrm{NH}}$	$\frac{1}{2}(J_{\mathrm{ND}}+J_{\mathrm{HD}})$
$\left\|1,1,\frac{1}{2}\right\rangle$	$\frac{1}{4}J_{\mathrm{NH}}$	$-\frac{1}{2}(J_{\mathrm{ND}}+J_{\mathrm{HD}})$
$\left\|0,1,\frac{1}{2}\right\rangle$	$\frac{1}{4}J_{\mathrm{NH}}$	$-(J_{\mathrm{ND}}+J_{\mathrm{HD}})$
$\left\|1,0,\frac{1}{2}\right\rangle$	$-\frac{3}{4}J_{\mathrm{NH}}$	0

Transition	Spectral frequency (high)
$\left\|3,2,\frac{3}{2}\right\rangle \rightarrow \left\|2,1,\frac{3}{2}\right\rangle$	$2J_{\mathrm{NH}}+\frac{3}{4}J_{\mathrm{ND}}+\frac{1}{4}J_{\mathrm{HD}}$
$\left\|2,2,\frac{3}{2}\right\rangle \rightarrow \left\|2,1,\frac{3}{2}\right\rangle$	$2J_{\mathrm{NH}}-2J_{\mathrm{HD}}$
$\left\|2,2,\frac{3}{2}\right\rangle \rightarrow \left\|1,1,\frac{3}{2}\right\rangle$	$2J_{\mathrm{NH}}-\frac{1}{2}J_{\mathrm{ND}}+\frac{1}{2}J_{\mathrm{HD}}$
$\left\|1,2,\frac{3}{2}\right\rangle \rightarrow \left\|2,1,\frac{3}{2}\right\rangle$	$2J_{\mathrm{NH}}-\frac{1}{2}J_{\mathrm{ND}}-\frac{7}{2}J_{\mathrm{HD}}$
$\left\|1,2,\frac{3}{2}\right\rangle \rightarrow \left\|1,1,\frac{3}{2}\right\rangle$	$2J_{\mathrm{NH}}-J_{\mathrm{ND}}-J_{\mathrm{HD}}$
$\left\|1,2,\frac{3}{2}\right\rangle \rightarrow \left\|0,1,\frac{3}{2}\right\rangle$	$2J_{\mathrm{NH}}-\frac{5}{4}J_{\mathrm{ND}}+\frac{1}{4}J_{\mathrm{HD}}$
$\left\|2,1,\frac{1}{2}\right\rangle \rightarrow \left\|1,0,\frac{1}{2}\right\rangle$	$J_{\mathrm{NH}}+\frac{1}{2}J_{\mathrm{ND}}+\frac{1}{2}J_{\mathrm{HD}}$
$\left\|1,1,\frac{1}{2}\right\rangle \rightarrow \left\|1,0,\frac{1}{2}\right\rangle$	$J_{\mathrm{NH}}-\frac{1}{2}J_{\mathrm{ND}}-\frac{1}{2}J_{\mathrm{HD}}$
$\left\|0,1,\frac{1}{2}\right\rangle \rightarrow \left\|1,0,\frac{1}{2}\right\rangle$	$2J_{\mathrm{NH}}-J_{\mathrm{ND}}-J_{\mathrm{HD}}$

Transition	Spectral frequency (low)
$\left\|3,2,\frac{3}{2}\right\rangle \rightarrow \left\|2,2,\frac{3}{2}\right\rangle$	$\frac{3}{4}J_{\mathrm{ND}}+\frac{9}{4}J_{\mathrm{HD}}$
$\left\|2,2,\frac{3}{2}\right\rangle \rightarrow \left\|1,2,\frac{3}{2}\right\rangle$	$\frac{1}{2}J_{\mathrm{ND}}+\frac{3}{2}J_{\mathrm{HD}}$

$$\left|1,1,\frac{3}{2}\right\rangle \rightarrow \left|0,1,\frac{3}{2}\right\rangle \qquad -\frac{1}{4}J_{\mathrm{ND}}+\frac{5}{4}J_{\mathrm{HD}}$$

$$\left|1,1,\frac{1}{2}\right\rangle \rightarrow \left|0,1,\frac{1}{2}\right\rangle \qquad \frac{1}{2}J_{\mathrm{ND}}+\frac{1}{2}J_{\mathrm{HD}}$$

A3. Analytical calculation of zero-field NMR spectrum of $^{15}ND_2H_2^+$

We use the same approach for calculating nuclear energy levels of the ion $^{15}\mathrm{ND_2H_2^+}$. However, here we have an additional degree of freedom since K_B can now take values 0, 1 and 2. States are denoted $|F, F_\mathrm{A}, K_\mathrm{A}\rangle$ and K_B is given explicitly (**Table A4**). One should note that perturbation theory will eventually break down for states with larger K_B (specifically, $K_\mathrm{B}=2$ in this case) since the corresponding term in the Hamiltonian increases. However, states with $K_\mathrm{B}=1$ are still approximated well by perturbation theory. The selection rules introduced above remain unchanged.

Table A4. Nuclear spin eigenstates, corresponding energies, allowed transitions and zero-field NMR spectral frequencies of $^{15}\mathrm{ND_2H_2^+}$ ion.

K_B	Eigenstate, $\lvert F, F_\mathrm{A}, K_\mathrm{A}\rangle$	E_0	E_1
0	$\left\lvert\frac{3}{2},\frac{3}{2},1\right\rangle$	$\frac{1}{2}J_{\mathrm{NH}}$	0
	$\left\lvert\frac{1}{2},\frac{1}{2},0\right\rangle$	0	0
1	$\left\lvert\frac{5}{2},\frac{3}{2},1\right\rangle$	$\frac{1}{2}J_{\mathrm{NH}}$	$\frac{1}{2}(J_{\mathrm{ND}}+2J_{\mathrm{HD}})$
	$\left\lvert\frac{3}{2},\frac{3}{2},1\right\rangle$	$\frac{1}{2}J_{\mathrm{NH}}$	$-\frac{1}{3}(J_{\mathrm{ND}}+2J_{\mathrm{HD}})$
	$\left\lvert\frac{1}{2},\frac{3}{2},1\right\rangle$	$\frac{1}{2}J_{\mathrm{NH}}$	$-\frac{5}{6}(J_{\mathrm{ND}}+2J_{\mathrm{HD}})$
	$\left\lvert\frac{3}{2},\frac{1}{2},1\right\rangle$	$-J_{\mathrm{NH}}$	$-\frac{1}{6}(J_{\mathrm{ND}}-4J_{\mathrm{HD}})$

	$\left\|\frac{1}{2},\frac{1}{2},1\right\rangle$	$-J_{\mathrm{NH}}$	$\frac{1}{3}(J_{\mathrm{ND}}-4J_{\mathrm{HD}})$
	$\left\|\frac{3}{2},\frac{1}{2},0\right\rangle$	0	$\frac{1}{2}J_{\mathrm{ND}}$
	$\left\|\frac{1}{2},\frac{1}{2},0\right\rangle$	0	$-J_{\mathrm{ND}}$
2	$\left\|\frac{7}{2},\frac{3}{2},1\right\rangle$	$\frac{1}{2}J_{\mathrm{NH}}$	$J_{\mathrm{ND}}+2J_{\mathrm{HD}}$
	$\left\|\frac{5}{2},\frac{3}{2},1\right\rangle$	$\frac{1}{2}J_{\mathrm{NH}}$	$-\frac{1}{6}(J_{\mathrm{ND}}+2J_{\mathrm{HD}})$
	$\left\|\frac{3}{2},\frac{3}{2},1\right\rangle$	$\frac{1}{2}J_{\mathrm{NH}}$	$-(J_{\mathrm{ND}}+2J_{\mathrm{HD}})$
	$\left\|\frac{1}{2},\frac{3}{2},1\right\rangle$	$\frac{1}{2}J_{\mathrm{NH}}$	$-\frac{3}{2}(J_{\mathrm{ND}}+2J_{\mathrm{HD}})$
	$\left\|\frac{5}{2},\frac{1}{2},1\right\rangle$	$-J_{\mathrm{NH}}$	$-\frac{1}{3}(J_{\mathrm{ND}}-4J_{\mathrm{HD}})$
	$\left\|\frac{3}{2},\frac{1}{2},1\right\rangle$	$-J_{\mathrm{NH}}$	$\frac{1}{2}(J_{\mathrm{ND}}-4J_{\mathrm{HD}})$
	$\left\|\frac{1}{2},\frac{1}{2},1\right\rangle$	$-J_{\mathrm{NH}}$	$(J_{\mathrm{ND}}+2J_{\mathrm{HD}})$
	$\left\|\frac{5}{2},\frac{1}{2},0\right\rangle$	0	J_{ND}
	$\left\|\frac{3}{2},\frac{1}{2},0\right\rangle$	0	$-\frac{3}{2}J_{\mathrm{ND}}$

K_{B}	Transition	Spectral frequency (high)
1	$\left\|\frac{5}{2},\frac{3}{2},1\right\rangle \rightarrow \left\|\frac{3}{2},\frac{1}{2},1\right\rangle$	$\frac{3}{2}J_{\mathrm{NH}}+\frac{2}{3}J_{\mathrm{ND}}+\frac{1}{3}J_{\mathrm{HD}}$
	$\left\|\frac{3}{2},\frac{3}{2},1\right\rangle \rightarrow \left\|\frac{3}{2},\frac{1}{2},1\right\rangle$	$\frac{3}{2}J_{\mathrm{NH}}-\frac{1}{6}J_{\mathrm{ND}}-\frac{4}{3}J_{\mathrm{HD}}$
	$\left\|\frac{3}{2},\frac{3}{2},1\right\rangle \rightarrow \left\|\frac{1}{2},\frac{1}{2},1\right\rangle$	$\frac{3}{2}J_{\mathrm{NH}}-\frac{2}{3}J_{\mathrm{ND}}+\frac{2}{3}J_{\mathrm{HD}}$
	$\left\|\frac{1}{2},\frac{3}{2},1\right\rangle \rightarrow \left\|\frac{1}{2},\frac{1}{2},1\right\rangle$	$\frac{3}{2}J_{\mathrm{NH}}-\frac{7}{6}J_{\mathrm{ND}}-\frac{1}{3}J_{\mathrm{HD}}$

2	$\left\|\frac{7}{2},\frac{3}{2},1\right\rangle \rightarrow \left\|\frac{5}{2},\frac{1}{2},1\right\rangle$	$\frac{3}{2}J_{\mathrm{NH}}+\frac{4}{3}J_{\mathrm{ND}}+\frac{2}{3}J_{\mathrm{HD}}$
	$\left\|\frac{5}{2},\frac{3}{2},1\right\rangle \rightarrow \left\|\frac{5}{2},\frac{1}{2},1\right\rangle$	$\frac{3}{2}J_{\mathrm{NH}}+\frac{1}{6}J_{\mathrm{ND}}-\frac{5}{3}J_{\mathrm{HD}}$
	$\left\|\frac{5}{2},\frac{3}{2},1\right\rangle \rightarrow \left\|\frac{3}{2},\frac{1}{2},1\right\rangle$	$\frac{3}{2}J_{\mathrm{NH}}-\frac{2}{3}J_{\mathrm{ND}}+\frac{5}{3}J_{\mathrm{HD}}$
	$\left\|\frac{3}{2},\frac{3}{2},1\right\rangle \rightarrow \left\|\frac{5}{2},\frac{1}{2},1\right\rangle$	$\frac{3}{2}J_{\mathrm{NH}}-\frac{2}{3}J_{\mathrm{ND}}-\frac{10}{3}J_{\mathrm{HD}}$
	$\left\|\frac{3}{2},\frac{3}{2},1\right\rangle \rightarrow \left\|\frac{3}{2},\frac{1}{2},1\right\rangle$	$\frac{3}{2}J_{\mathrm{NH}}-\frac{3}{2}J_{\mathrm{ND}}$
	$\left\|\frac{3}{2},\frac{3}{2},1\right\rangle \rightarrow \left\|\frac{1}{2},\frac{1}{2},1\right\rangle$	$\frac{3}{2}J_{\mathrm{NH}}-2J_{\mathrm{ND}}+2J_{\mathrm{HD}}$
	$\left\|\frac{1}{2},\frac{3}{2},1\right\rangle \rightarrow \left\|\frac{3}{2},\frac{1}{2},1\right\rangle$	$\frac{3}{2}J_{\mathrm{NH}}-2J_{\mathrm{ND}}-J_{\mathrm{HD}}$
	$\left\|\frac{1}{2},\frac{3}{2},1\right\rangle \rightarrow \left\|\frac{1}{2},\frac{1}{2},1\right\rangle$	$\frac{3}{2}J_{\mathrm{NH}}-\frac{5}{2}J_{\mathrm{ND}}+J_{\mathrm{HD}}$

K_{B}	Transition	Spectral frequency (low)
1	$\left\|\frac{5}{2},\frac{3}{2},1\right\rangle \rightarrow \left\|\frac{3}{2},\frac{3}{2},1\right\rangle$	$\frac{5}{6}J_{\mathrm{ND}}+\frac{5}{3}J_{\mathrm{HD}}$
	$\left\|\frac{3}{2},\frac{3}{2},1\right\rangle \rightarrow \left\|\frac{1}{2},\frac{3}{2},1\right\rangle$	$\frac{1}{2}J_{\mathrm{ND}}+J_{\mathrm{HD}}$
	$\left\|\frac{3}{2},\frac{1}{2},1\right\rangle \rightarrow \left\|\frac{1}{2},\frac{1}{2},1\right\rangle$	$-\frac{1}{2}J_{\mathrm{ND}}+2J_{\mathrm{HD}}$
	$\left\|\frac{3}{2},\frac{1}{2},0\right\rangle \rightarrow \left\|\frac{1}{2},\frac{1}{2},0\right\rangle$	$\frac{3}{2}J_{\mathrm{ND}}$
2	$\left\|\frac{7}{2},\frac{3}{2},1\right\rangle \rightarrow \left\|\frac{5}{2},\frac{3}{2},1\right\rangle$	$\frac{7}{6}J_{\mathrm{ND}}+\frac{7}{3}J_{\mathrm{HD}}$
	$\left\|\frac{5}{2},\frac{3}{2},1\right\rangle \rightarrow \left\|\frac{3}{2},\frac{3}{2},1\right\rangle$	$\frac{5}{6}J_{\mathrm{ND}}+\frac{5}{3}J_{\mathrm{HD}}$
	$\left\|\frac{3}{2},\frac{3}{2},1\right\rangle \rightarrow \left\|\frac{1}{2},\frac{3}{2},1\right\rangle$	$\frac{1}{2}J_{\mathrm{ND}}+J_{\mathrm{HD}}$
	$\left\|\frac{5}{2},\frac{1}{2},1\right\rangle \rightarrow \left\|\frac{3}{2},\frac{1}{2},1\right\rangle$	$-\frac{5}{6}J_{\mathrm{ND}}+\frac{10}{3}J_{\mathrm{HD}}$

$$\left|\frac{3}{2},\frac{1}{2},1\right\rangle \rightarrow \left|\frac{1}{2},\frac{1}{2},1\right\rangle \qquad -\frac{1}{2}J_{\mathrm{ND}}+2J_{\mathrm{HD}}$$

$$\left|\frac{5}{2},\frac{1}{2},0\right\rangle \rightarrow \left|\frac{3}{2},\frac{1}{2},0\right\rangle \qquad \frac{5}{2}J_{\mathrm{ND}}$$

A3. Analytical calculation of zero-field NMR spectrum of $^{15}ND_3H^+$

Analogously, we derive energy levels and corresponding transitions for the $^{15}ND_3H^+$ ion. One may note that actual frequencies may deviate from the derived ones due to the fact that perturbation theory no longer holds for large K_B values.

Table A5. Nuclear spin eigenstates, corresponding energies, allowed transitions and zero-field NMR spectral frequencies of $^{15}ND_3H^+$ ion.

K_B	Eigenstate, $\|F, K_B, F_A\rangle$	E_0	E_1
0	$\|4,3,1\rangle$	$\frac{1}{4}J_{\mathrm{NH}}$	$\frac{3}{2}J_{\mathrm{ND}}+\frac{3}{2}J_{\mathrm{HD}}$
	$\|3,3,1\rangle$	$\frac{1}{4}J_{\mathrm{NH}}$	$-\frac{1}{2}J_{\mathrm{ND}}-\frac{1}{2}J_{\mathrm{HD}}$
	$\|2,3,1\rangle$	$\frac{1}{4}J_{\mathrm{NH}}$	$-2J_{\mathrm{ND}}-2J_{\mathrm{HD}}$
	$\|3,2,1\rangle$	$\frac{1}{4}J_{\mathrm{NH}}$	$J_{\mathrm{ND}}+J_{\mathrm{HD}}$
	$\|2,2,1\rangle$	$\frac{1}{4}J_{\mathrm{NH}}$	$-\frac{1}{2}J_{\mathrm{ND}}-\frac{1}{2}J_{\mathrm{HD}}$
	$\|1,2,1\rangle$	$\frac{1}{4}J_{\mathrm{NH}}$	$-\frac{3}{2}J_{\mathrm{ND}}-\frac{3}{2}J_{\mathrm{HD}}$
	$\|2,1,1\rangle$	$\frac{1}{4}J_{\mathrm{NH}}$	$\frac{1}{2}J_{\mathrm{ND}}+\frac{1}{2}J_{\mathrm{HD}}$
	$\|1,1,1\rangle$	$\frac{1}{4}J_{\mathrm{NH}}$	$-\frac{1}{2}J_{\mathrm{ND}}-\frac{1}{2}J_{\mathrm{HD}}$
	$\|0,1,1\rangle$	$\frac{1}{4}J_{\mathrm{NH}}$	$-J_{\mathrm{ND}}-J_{\mathrm{HD}}$

$\|1,0,1\rangle$	$\frac{1}{4}J_{\mathrm{NH}}$	0
$\|3,3,0\rangle$	$-\frac{3}{4}J_{\mathrm{NH}}$	0
$\|2,2,0\rangle$	$-\frac{3}{4}J_{\mathrm{NH}}$	0
$\|1,1,0\rangle$	$-\frac{3}{4}J_{\mathrm{NH}}$	0
$\|0,0,0\rangle$	$-\frac{3}{4}J_{\mathrm{NH}}$	0

Transition	Spectral frequency (high)
$\|4,3,1\rangle \rightarrow \|3,3,0\rangle$	$J_{\mathrm{NH}} + \frac{3}{2}J_{\mathrm{ND}} + \frac{3}{2}J_{\mathrm{HD}}$
$\|3,3,1\rangle \rightarrow \|3,3,0\rangle$	$J_{\mathrm{NH}} - \frac{1}{2}J_{\mathrm{ND}} - \frac{1}{2}J_{\mathrm{HD}}$
$\|2,3,1\rangle \rightarrow \|3,3,0\rangle$	$J_{\mathrm{NH}} - 2J_{\mathrm{ND}} - 2J_{\mathrm{HD}}$
$\|3,2,1\rangle \rightarrow \|2,2,0\rangle$	$J_{\mathrm{NH}} + J_{\mathrm{ND}} + J_{\mathrm{HD}}$
$\|2,2,1\rangle \rightarrow \|2,2,0\rangle$	$J_{\mathrm{NH}} - \frac{1}{2}J_{\mathrm{ND}} - \frac{1}{2}J_{\mathrm{HD}}$
$\|1,2,1\rangle \rightarrow \|2,2,0\rangle$	$J_{\mathrm{NH}} - \frac{3}{2}J_{\mathrm{ND}} - \frac{3}{2}J_{\mathrm{HD}}$
$\|2,1,1\rangle \rightarrow \|1,1,0\rangle$	$J_{\mathrm{NH}} + \frac{1}{2}J_{\mathrm{ND}} + \frac{1}{2}J_{\mathrm{HD}}$
$\|1,1,1\rangle \rightarrow \|1,1,0\rangle$	$J_{\mathrm{NH}} - \frac{1}{2}J_{\mathrm{ND}} - \frac{1}{2}J_{\mathrm{HD}}$
$\|0,1,1\rangle \rightarrow \|1,1,0\rangle$	$J_{\mathrm{NH}} - J_{\mathrm{ND}} - J_{\mathrm{HD}}$

Transition	Spectral frequency (high)
$\|4,3,1\rangle \rightarrow \|3,3,1\rangle$	$2J_{\mathrm{ND}} + 2J_{\mathrm{HD}}$
$\|3,3,1\rangle \rightarrow \|2,3,1\rangle$	$\frac{3}{2}J_{\mathrm{ND}} + \frac{3}{2}J_{\mathrm{HD}}$

$\|3,2,1\rangle \rightarrow \|2,2,1\rangle$	$\frac{3}{2}J_{\mathrm{ND}} + \frac{3}{2}J_{\mathrm{HD}}$
$\|3,2,1\rangle \rightarrow \|2,2,1\rangle$	$J_{\mathrm{ND}} + J_{\mathrm{HD}}$
$\|3,2,1\rangle \rightarrow \|2,2,1\rangle$	$J_{\mathrm{ND}} + J_{\mathrm{HD}}$
$\|3,2,1\rangle \rightarrow \|2,2,1\rangle$	$\frac{1}{2}J_{\mathrm{ND}} + \frac{1}{2}J_{\mathrm{HD}}$

A4. Analytical calculation of zero-field NMR spectrum of $^{15}ND_4^+$

For $^{15}ND_4^+$ ($x = 4$) the spectrum may be solved analytically without the use of perturbation theory. The Hamiltonian is given by

$$\widehat{H} = J_{\mathrm{ND}}(\widehat{\mathbf{S}} \cdot \widehat{\mathbf{K}}_{\mathrm{B}}). \tag{A9}$$

The selection rules introduced above remain unchanged, but $\widehat{\mathbf{K}}_{\mathrm{A}}$ is now replaced by $\widehat{\mathbf{K}}_{\mathrm{B}}$. We therefore obtain the states and transitions shown in **Table A6**. States are denoted as $|F, K_{\mathrm{B}}\rangle$, here F is the quantum number corresponding to $\widehat{\mathbf{F}} = \widehat{\mathbf{S}} + \widehat{\mathbf{K}}_{\mathrm{B}}$.

Table A6. Nuclear spin eigenstates, corresponding energies, allowed transitions and zero-field NMR spectral frequencies of $^{15}ND_4^+$ ion.

Eigenstate, $\|F_{\mathrm{A}}, K_{\mathrm{A}}\rangle$	Energy	Transition	Spectral frequency
$\left\|\frac{9}{2}, 4\right\rangle$	$2J_{\mathrm{ND}}$	$\left\|\frac{9}{2}, 4\right\rangle \rightarrow \left\|\frac{7}{2}, 4\right\rangle$	$\frac{9}{2}J_{\mathrm{ND}}$
$\left\|\frac{7}{2}, 4\right\rangle$	$-\frac{5}{2}J_{\mathrm{ND}}$	$\left\|\frac{7}{2}, 3\right\rangle \rightarrow \left\|\frac{5}{2}, 3\right\rangle$	$\frac{7}{2}J_{\mathrm{ND}}$
$\left\|\frac{7}{2}, 3\right\rangle$	$\frac{3}{2}J_{\mathrm{ND}}$	$\left\|\frac{5}{2}, 2\right\rangle \rightarrow \left\|\frac{3}{2}, 2\right\rangle$	$\frac{5}{2}J_{\mathrm{ND}}$
$\left\|\frac{5}{2}, 3\right\rangle$	$-2J_{\mathrm{ND}}$	$\left\|\frac{3}{2}, 1\right\rangle \rightarrow \left\|\frac{1}{2}, 1\right\rangle$	$\frac{3}{2}J_{\mathrm{ND}}$
$\left\|\frac{5}{2}, 2\right\rangle$	J_{ND}		

$\left\|\frac{3}{2},2\right\rangle$	$-\frac{3}{2}J_{\mathrm{ND}}$
$\left\|\frac{3}{2},1\right\rangle$	$\frac{1}{2}J_{\mathrm{ND}}$
$\left\|\frac{1}{2},1\right\rangle$	$-J_{\mathrm{ND}}$
$\left\|\frac{1}{2},0\right\rangle$	0

Acknowledgments

We gratefully acknowledge the financial support by NSF CHE-1709944, funding from the European Union's Horizon 2020 research, and Alexander von Humboldt Foundation in the framework of the Sofja Kovalevskaja Award. DB acknowledges support by the Cluster of Excellence Precision Physics, Fundamental Interactions, and Structure of Matter (PRISMA+ EXC 2118/1) funded by the DFG within the German Excellence Strategy (Project ID 39083149).

References

1. Ledbetter, M. P.; Savukov, I. M.; Budker, D.; Shah, V.; Knappe, S.; Kitching, J.; Michalak, D. J.; Xu, S.; Pines, A., Zero-field remote detection of NMR with a microfabricated atomic magnetometer. *Proceedings of the National Academy of Sciences* **2008,** *105* (7), 2286-2290.

2. Ledbetter, M. P.; Crawford, C. W.; Pines, A.; Wemmer, D. E.; Knappe, S.; Kitching, J.; Budker, D., Optical detection of NMR J-spectra at zero magnetic field. *J. Magn. Reson.* **2009,** *199* (1), 25-29.

3. Ledbetter, M. P.; Theis, T.; Blanchard, J. W.; Ring, H.; Ganssle, P.; Appelt, S.; Blümich, B.; Pines, A.; Budker, D., Near-Zero-Field Nuclear Magnetic Resonance. *Phys. Rev. Lett.* **2011,** *107* (10), 107601.

4. Blanchard, J. W.; Ledbetter, M. P.; Theis, T.; Butler, M. C.; Budker, D.; Pines, A., High-Resolution Zero-Field NMR J-Spectroscopy of Aromatic Compounds. *J. Am. Chem. Soc.* **2013,** *135* (9), 3607-3612.

5. Blanchard, J. W.; Budker, D., Zero- to Ultralow-field NMR. *Emagres* **2016,** *5* (3), 1395-1409.

6. Tayler, M. C. D.; Theis, T.; Sjolander, T. F.; Blanchard, J. W.; Kentner, A.; Pustelny, S.; Pines, A.; Budker, D., Invited Review Article: Instrumentation for nuclear magnetic resonance in zero and ultralow magnetic field. *Rev. Sci. Instrum.* **2017,** *88* (9), 091101.

7. Budker, D.; Romalis, M., Optical magnetometry. *Nat. Phys.* **2007,** *3* (4), 227-234.

8. Budker, D., Extreme nuclear magnetic resonance: Zero field, single spins, dark matter…. *J. Magn. Reson.* **2019**.

9. Barskiy, D. A.; Tayler, M. C. D.; Marco-Rius, I.; Kurhanewicz, J.; Vigneron, D. B.; Cikrikci, S.; Aydogdu, A.; Reh, M.; Pravdivtsev, A. N.; Hövener, J.-B.; Blanchard, J. W.; Wu, T.; Budker, D.; Pines, A., Zero-field nuclear magnetic resonance of chemically exchanging systems. *Nat. Commun.* **2019,** *10* (1), 3002.

10. Burueva, D. B.; Eills, J.; Blanchard, J. W.; Garcon, A.; Picazo-Frutos, R.; Kovtunov, K. V.; Koptyug, I. V.; Budker, D., Chemical Reaction Monitoring using Zero-Field Nuclear Magnetic Resonance Enables Study of Heterogeneous Samples in Metal Containers. *Angewandte Chemie International Edition* **2020,** *59* (39), 17026-17032.

11. Pustelny, S.; Jackson Kimball, D. F.; Pankow, C.; Ledbetter, M. P.; Wlodarczyk, P.; Wcislo, P.; Pospelov, M.; Smith, J. R.; Read, J.; Gawlik, W.; Budker, D., The Global Network of Optical Magnetometers for Exotic physics (GNOME): A novel scheme to search for physics beyond the Standard Model. *Annalen der Physik* **2013,** *525* (8-9), 659-670.

12. Levitt, M. H., Spin Dynamics: Basics of Nuclear Magnetic Resonance. **2008**.

13. Sjolander, T. F. Advances in Pulsed Zero-Field NMR. University of California, Berkeley, USA, 2017.

14. Tayler, M. C. D.; Gladden, L. F., Scalar relaxation of NMR transitions at ultralow magnetic field. *J. Magn. Reson.* **2019,** *298*, 101-106.

15. Sjolander, T. F.; Tayler, M. C. D.; King, J. P.; Budker, D.; Pines, A., Transition-Selective Pulses in Zero-Field Nuclear Magnetic Resonance. *J. Phys. Chem. A* **2016,** *120* (25), 4343-4348.

16. Tayler, M. C. D.; Ward-Williams, J.; Gladden, L. F., NMR relaxation in porous materials at zero and ultralow magnetic fields. *J. Magn. Reson.* **2018,** *297*, 1-8.

17. Halle, B.; Denisov, V. P., Magnetic relaxation dispersion studies of biomolecular solutions. *Methods Enzymol.* **2001,** *338* (Nuclear Magnetic Resonance of Biological Macromolecules, Part A), 178-201.

18. Kowalewski, J.; Mäler, L., Nuclear Spin Relaxation in Liquids: Theory, Experiments, and Applications. In *Series in Chemical Physics*, Moore, H. J.; Spencer, N. D., Eds. CRC Press Taylor & Francis Group Boca Raton, FL. , 2006; Vol. 2, p 426

19. Blanchard, J. W. Zero and Ultra-Low-Field Nuclear Magnetic Resonance Spectroscopy Via Optical Magnetometry. University of California at Berkeley, 2014.

20. Stone, N. J., Table of nuclear magnetic dipole and electric quadrupole moments. *Atomic Data and Nuclear Data Tables* **2005,** *90* (1), 75-176.

21. Ramsey, N. F., Electron Coupled Interactions between Nuclear Spins in Molecules. *Phys. Rev.* **1953,** *91* (2), 303-307.

22. Del Bene, J. E.; Elguero, J., Predicted Signs of One-Bond Spin−Spin Coupling Constants (1hJH-Y) across X−H−Y Hydrogen Bonds for Complexes with Y = 15N, 17O, and 19F. *J. Phys. Chem. A* **2004,** *108* (52), 11762-11767.

23. King, J. P.; Sjolander, T. F.; Blanchard, J. W., Antisymmetric Couplings Enable Direct Observation of Chirality in Nuclear Magnetic Resonance Spectroscopy. *J. Phys. Chem. Lett.* **2017,** *8* (4), 710-714.

24. Blanchard, J. W.; King, J. P.; Sjolander, T. F.; Kozlov, M. G.; Budker, D., Molecular parity nonconservation in nuclear spin couplings. *Physical Review Research* **2020,** *2* (2), 023258.

25. Mata, R. A.; Suhm, M. A., Benchmarking Quantum Chemical Methods: Are We Heading in the Right Direction? *Angewandte Chemie International Edition* **2017,** *56* (37), 11011-11018.

26. Wilzewski, A.; Afach, S.; Blanchard, J. W.; Budker, D., A method for measurement of spin-spin couplings with sub-mHz precision using zero- to ultralow-field nuclear magnetic resonance. *J. Magn. Reson.* **2017,** *284*, 66-72.

27. Grunwald, E.; Ku, A. Y., Proton exchange between ammonium ion, trimethyl-ammonium ion, and water. Speed of the dehydration step that precedes bimolecular proton transfer. *J. Am. Chem. Soc.* **1968,** *90* (1), 29-31.

28. Butler, M. C.; Ledbetter, M. P.; Theis, T.; Blanchard, J. W.; Budker, D.; Pines, A., Multiplets at zero magnetic field: The geometry of zero-field NMR. *The Journal of Chemical Physics* **2013,** *138* (18), 184202.

29. Abragam, A., *The principles of nuclear magnetism*. Clarendon Press: Oxford, 1961.

30. Chiavazza, E.; Kubala, E.; Gringeri, C. V.; Düwel, S.; Durst, M.; Schulte, R. F.; Menzel, M. I., Earth's magnetic field enabled scalar coupling relaxation of 13C nuclei bound to fast-relaxing quadrupolar 14N in amide groups. *J. Magn. Reson.* **2013,** *227*, 35-38.

31. Ivanov, K. L.; Kress, T.; Baudin, M.; Guarin, D.; Abergel, D.; Bodenhausen, G.; Kurzbach, D., Relaxation of long-lived modes in NMR of deuterated methyl groups. *The Journal of chemical physics* **2018,** *149* (5), 054202.

32. Meier, B.; Dumez, J. N.; Stevanato, G.; Hill-Cousins, J. T.; Roy, S. S.; Hakansson, P.; Mamone, S.; Brown, R. C. D.; Pileio, G.; Levitt, M. H., Long-Lived Nuclear Spin States in Methyl Groups and Quantum-Rotor-Induced Polarization. *J. Am. Chem. Soc.* **2013,** *135* (50), 18746-18749.

33. Dumez, J. N.; Hakansson, P.; Mamone, S.; Meier, B.; Stevanato, G.; Hill-Cousins, J. T.; Roy, S. S.; Brown, R. C. D.; Pileio, G.; Levitt, M. H., Theory of long-lived nuclear spin states in methyl groups and quantum-rotor induced polarisation. *J. Chem. Phys.* **2015,** *142* (4), 044506.

34. Sarkar, R.; Ahuja, P.; Vasos, P. R.; Bornet, A.; Wagnieres, O.; Bodenhausen, G., Long-lived coherences for line-narrowing in high-field NMR. *Prog. Nucl. Magn. Reson. Spectrosc.* **2011,** *59* (1), 83-90.

35. Emondts, M.; Ledbetter, M. P.; Pustelny, S.; Theis, T.; Patton, B.; Blanchard, J. W.; Butler, M. C.; Budker, D.; Pines, A., Long-Lived Heteronuclear Spin-Singlet States in Liquids at a Zero Magnetic field. *Phys. Rev. Lett.* **2014,** *112* (7), 077601.

36. Kiryutin, A. S.; Zhukov, I. V.; Yurkovskaya, A. V.; Budker, D.; Ivanov, K. L., Chapter 23 Singlet Order in Heteronuclear Spin Systems. In *Long-lived Nuclear Spin Order: Theory and Applications*, The Royal Society of Chemistry: 2020; pp 418-433.

37. Iali, W.; Rayner, P. J.; Duckett, S. B., Using parahydrogen to hyperpolarize amines, amides, carboxylic acids, alcohols, phosphates, and carbonates. *Science Advances* **2018,** *4*.

38. Iali, W.; Rayner, P. J.; Alshehri, A.; Holmes, A. J.; Ruddlesden, A. J.; Duckett, S. B., Direct and indirect hyperpolarisation of amines using para hydrogen. *Chemical science* **2018,** *9* (15), 3677-3684.

39. Sarkar, R.; Comment, A.; Vasos, P. R.; Jannin, S.; Gruetter, R.; Bodenhausen, G.; Hall, H.; Kirik, D.; Denisov, V. P., Proton NMR of 15N-Choline Metabolites Enhanced by Dynamic Nuclear Polarization. *J. Am. Chem. Soc.* **2009,** *131* (44), 16014-16015.

40. Bowen, S.; Ardenkjaer-Larsen, J. H., Formulation and utilization of choline based samples for dissolution dynamic nuclear polarization. *J. Magn. Reson.* **2013,** *236*, 26-30.

41. Mao, J.; Jiang, L.; Jiang, B.; Liu, M.; Mao, X.-a., 1H–14N HSQC detection of choline-containing compounds in solutions. *J. Magn. Reson.* **2010,** *206* (1), 157-160.

42. Wall, E. M.; Woolley, S. C., Motor Performance: Acetylcholine in action. *eLife* **2020,** (9), e57515.

43. Mao, J.; Jiang, L.; Jiang, B.; Liu, M.; Mao, X.-a., A Selective NMR Method for Detecting Choline Containing Compounds in Liver Tissue: The 1H−14N HSQC Experiment. *J. Am. Chem. Soc.* **2010,** *132* (49), 17349-17351.

44. Mao, X.-a.; Li, N.; Mao, J.; Li, Q.; Xiao, N.; Jiang, B.; Jiang, L.; Wang, X.-x.; Liu, M., Fast detection of choline-containing metabolites in liver using 2D 1H–14N three-bond correlation (HN3BC) spectroscopy. *J. Magn. Reson.* **2012,** *214*, 352-359.

45. Hongsirikarn, K.; Goodwin, J. G.; Greenway, S.; Creager, S., Influence of ammonia on the conductivity of Nafion membranes. *J. Power Sources* **2010,** *195* (1), 30-38.